Supporting Information

A Monolithically Integrated, Intrinsically Safe, 10% Efficient, Solar-Driven Water-Splitting System Based on Active, Stable Earth-Abundant Electrocatalysts in Conjunction with Tandem III-V Light Absorbers Protected by Amorphous TiO_2 Films

Erik Verlage,[a,b] *Shu Hu,*[a,c] *Rui Liu,*[a] *Ryan J. R. Jones,*[a] *Ke Sun,*[a,c]

Chengxiang Xiang,[a]* *Nathan S. Lewis,*[a,c]* *Harry A. Atwater*[a,b]*

[a] Joint Center for Artificial Photosynthesis (JCAP)
California Institute of Technology
Pasadena, CA, 91125

[b] Department of Applied Physics and Materials Science
California Institute of Technology
Pasadena, CA, 91125

[c] Division of Chemistry and Chemical Engineering
California Institute of Technology
Pasadena, CA, 91125

*To whom correspondence should be addressed: haa@caltech.edu, nslewis@caltech.edu and cxx@caltech.edu

Materials and Methods

Chemicals and materials

All materials were used as received, except where otherwise noted. H_2O with a resistivity of 18.2 MΩ·cm was obtained from a Millipore de-ionized water system. A 1.0 M aqueous solution of KOH (semiconductor grade, Sigma-Aldrich, 99.99% trace metal basis) was prepared for all electrochemical measurements. Inlet and outlet ports (PEEK, 0.30" ID and 0.0625" OD) used in prototypes were purchased from Upchurch Scientific (Oak Harbor, WA 98277). The Ag-based conductive epoxy was obtained from CircuitWorks from ITW Chemtronics (Kennesaw, GA 30152).

Growth and preparation of III-V surfaces

The dual junction device was grown commercially (Sumika Electronic Materials, Inc.) according to specifications determined by 1-D numerical simulation using Helmholtz-Zentrum Berlin's AFORS-HET software. Planar III-V layers were grown epitaxially by metal-organic chemical vapour deposition (MOCVD) on an n^+-GaAs wafer with a (100)-oriented polished surface (Si-doped, acceptor concentration of 1×10^{19} cm^{-3}, 6" diameter).

Atomic layer deposition (ALD)

Films were deposited on the exposed p^+-GaAs epilayer at 150 °C using an Ultratech Fiji 200 plasma atomic-layer deposition (ALD) system. Prior to ALD, the epitaxial surface was immersed for 30 s in 1.0 M KOH (aqueous solution of potassium hydroxide pellets, semiconductor grade, 99.99% trace metals basis, Sigma-Aldrich),

rinsed with copious amounts of deionized H_2O, dried using a stream of N_2(g), and loaded immediately thereafter into the ALD chamber. Each ALD cycle consisted of a 0.06 s pulse of H_2O (18 MΩ · cm resistivity, Millipore), followed by a 0.25 s pulse of tetrakis(dimethylamido)titanium (TDMAT, Sigma-Aldrich, 99.999%, used as received). A 15 s purge under a constant 0.13 L min^{-1} flow of research-grade Ar (g) was performed between each precursor pulse. The base pressure during the TiO_2 growth was maintained at ~0.1 Torr. ALD-TiO_2 films with thicknesses of 62.5 nm and 150 nm were used to protect III-V surfaces.

Deposition of metal films and electrocatalysts

Ohmic contact to the n^+-GaAs wafer was formed using a Ge-Au eutectic (20 nm Ge/ 30 nm Au/ 15 nm Ni/ 100 nm Au) deposited by radio-frequency (RF) sputtering and annealed under N_2(g) at 400 °C for 30 s using rapid thermal annealing. Solid-state devices were formed by RF sputtering a metal grid of 100 nm thick Ni onto the p^+-GaAs surface. For all photoanode surfaces, an optically transparent nominally 2 nm thick Ni film was deposited on TiO_2 using RF sputtering. Counter electrodes were formed by drop casting Ni-Mo nanoparticles on Ni foil and annealing under forming gas (5% H_2, 95% N_2, 500 sccm, Airliquide) at 450 °C for 30 min, then cooling the electrodes to room temperature under forming gas.[1] For the fully integrated prototype, a Ti/Ni-Mo electrocatalyst was deposited using RF sputtering onto the Au-Ge back contact.

PEC assembly and device preparation

To measure the current density during photoelectrochemical operation, wafers were cleaved into samples 0.5~1 cm^2 in area, and samples were mounted onto a Cu film using a Ag-based conductive epoxy. Samples were then assembled into custom-made

compression cells that were equipped with fluorosilicone O-rings (0.0314 cm^2 Teflon, 0.34 cm^2 polymethyl methacrylate).

The prototype (Fig. 4a) consisted of: 1x PEC assemblies (10.0 mm x 10.0 mm), 2 x AHA-type NEOSEPTA anion exchange membrane (2 x 10 mm), 2 x acrylic chassis that were 3-D printed, 1 x quartz window (15 mm in diameter), 8 x inlet and outlet ports (PEEK, ID 0.75 mm, OD 1.5875 mm), and 16 x bolts (2-56" x 1") and/or epoxy (Loctite 9460, Hysol).

All transparent sections of the compression cells were covered using high-performance black masking tape purchased from Thorlabs to prevent illumination of electrochemically inactive surfaces.

AM 1.5 illumination and spectral response

A Xe lamp-based solar simulator and probe station was used to measure the solid-state device performance. The light intensity was adjusted based on an NREL-calibrated Si photovoltaic reference cell. For photoelectrochemical experiments, the illumination intensity was calibrated by placing a Si photodiode (Thor Labs) in the Teflon compression cell, in the same location occupied by the exposed area of the photoelectrode. The Si photodiode was previously calibrated by measurement of the short-circuit current-density value under AM 1.5 simulated sunlight at 100 mW cm^{-2} (1-Sun) of irradiance from a Xe arc lamp with an AM 1.5 filter. To obtain spectral response data, monochromatic light was chopped at 17 Hz and was focused onto the sample surface. An unchopped light-emitting diode (LED) was used to saturate the AlGaAs/GaAs heterojunction (850 nm) or the InGaP homojunction (405 nm), to measure the external quantum yield of the unsaturated subcell. Photoelectrochemical spectral response data were obtained at the formal potential for water oxidation using a side-facing chassis with a 0.34 cm^2 O-ring.

106

107 Electrochemical measurements

108

109 A saturated calomel electrode (SCE, CH Instruments) was used as a reference
110 electrode for all three-electrode photoelectrochemical measurements, including spectral
111 response data. The pH of the 1.0 M KOH(aq) solution was 13.7, as measured using a
112 VWR SympHony SB70P Digital, Bench-model pH Meter. The equilibrium potential for
113 water oxidation in 1.0 M KOH(aq) was calculated to be 0.18 V vs. SCE. The active cell
114 area was determined by the size of the O-ring. For stability tests the custom-built Teflon
115 compression cell (Fig. 2b) O-ring size was 0.031 cm^2, and a liquid pumping system was
116 used to facilitate removal of bubbles from the sample surface and to decrease mass
117 transfer effects. All data for three-electrode electrochemical measurements in aqueous
118 solutions included compensation for solution series resistance as obtained from high-
119 frequency electrical-impedance measurements.

120

121 Scanning electron microscopy (SEM) of device failure

122 For all samples, device failure was followed by a large increase in current density
123 caused by a breach in the TiO_2 protective film that led to photocorrosion of the III-V
124 layers. Lateral corrosion of the III-V device caused cracks in the TiO_2 that would
125 eventually lead to liftoff of the protection layer, as can be seen in Fig. S1a.

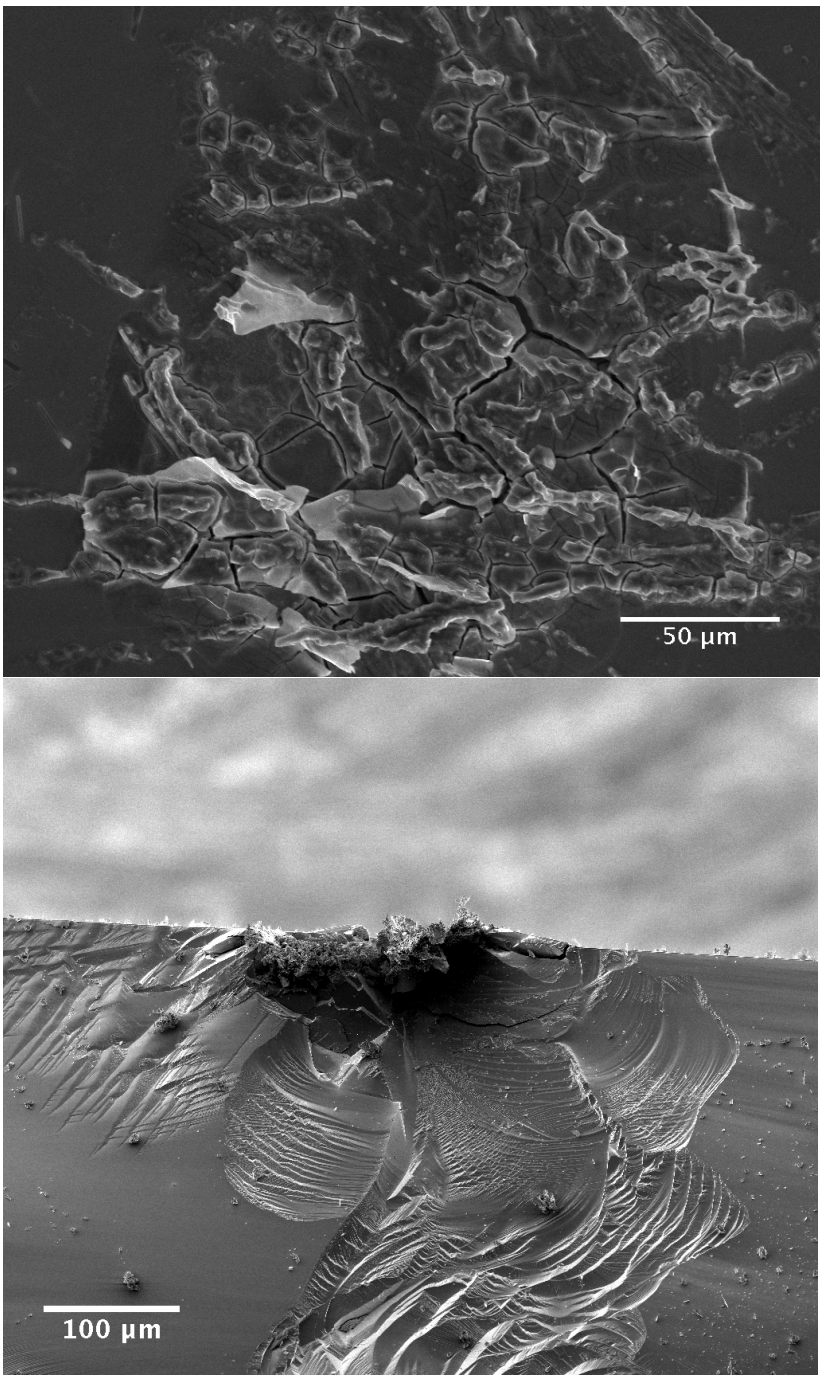

Figure S1 (a) SEM image of device failure after 6.5 hours of operation, showing cracking of ALD-TiO_2 protection layer and corrosion of underlying III-V semiconductors. (b) Side profile SEM of III-V corrosion.

Eudiometer gas collection

A custom-built polymethyl methacrylate (PMMA) chassis with anion exchange membrane partitions was used to separate the gas products. A system of Teflon tubing at the top of each chamber allowed H_2(g) and O_2(g) to flow into two eudiometers (0.05 mL precision) that were filled with de-ionized water and suspended over large water reservoirs. To prevent escape of hydrogen gas through the solution, the reservoir for H_2(g) collection was saturated with pure H_2(g) for 30 min before operation..

The gas collection apparatus for the fully integrated prototype is shown in Fig. 4b. The respective conduits transported gas products from the chassis chambers to the eudiometers (inverted burette geometry), terminating at the water reservoir level to insure that the chassis continuously operated at STP without any buildup of backpressure. High precision manometers (Extech HD755) were used to sample the pressure variation inside the eudiometers due to increasing gas volume every second. The pressure was measured in inches water column, resulting in a well-defined meniscus velocity during the experiment. A simple conversion factor between the eudiometer length and the eudiometer volume allowed determination of the gas production rate (ml/s) from measurement of the meniscus velocity (in/s). As produced gases were introduced to the inverted burette and the water level decreased, the pressure of the gases inside the burette increased. An additional conversion factor was applied to obtain the volume of produced gas at STP, which was used to obtain the solar-to-hydrogen conversion efficiency in Figure 4b.

The chassis in Figure 3a was also used for gas collection to determine the faradaic efficiency of the system, as shown in Figure S2. The current density from spontaneous water splitting was measured at zero external bias under 1.5 Sun illumination from a Xe arc lamp with an AM 1.5 filter. This system was used to calculate the expected gas production. Measurements were made at regular intervals for over a 5 h period. The Faradaic efficiency was 100% for O_2(g), and was 90% for H_2(g) collection, due to

hydrogen leaks in the chassis and tubing. The final products were analyzed using gas chromatography (GC) by thermal conductivity detectors (TCD), and the composition of the products was confirmed as well with a ~2% gas crossover rate.

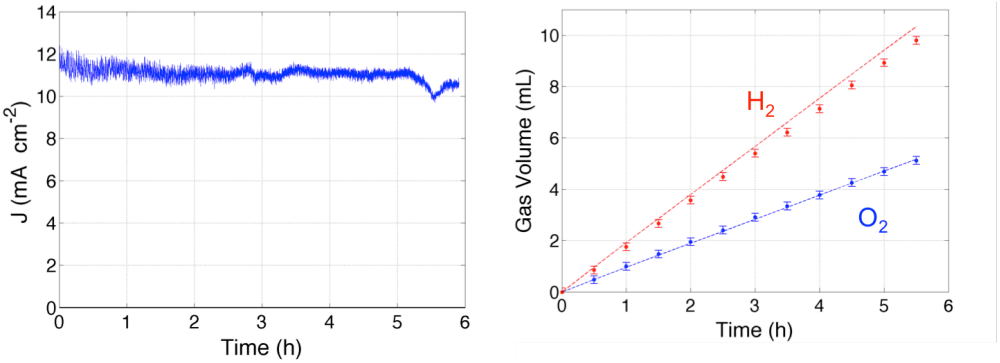

Figure S2 (a) Short-circuit photocurrent density $J_{photo,\ short}$ under 1.5 Suns using AM 1.5 illumination. (b) Gas volume was measured at regular intervals, and is compared to expected gas production (dotted lines) based on total charge passed.

Spectroscopic ellipsometry

Complex refractive index (n, k) data for films of as-grown TiO_2 on Si were obtained using spectroscopic ellipsometry. The ellipsometric data were acquired using a J.A. Woolam V-VASE system. The non-absorbing (k~0) portion of the data was fit using a Cauchy model that assumed a TiO_2/SiO_2 bilayer structure on Si. The TiO_2 n, k values were extracted from a point-by-point fit, using fixed Cauchy and film-thickness parameters.

Optical modeling

Reflection spectra of tandem III-V substrates with TiO_2 coatings of different thicknesses were calculated by solving the transfer matrix (Figure S3a). Refractive

indices of all the layers were obtained or interpolated from experimental data at http://www.ioffe.ru/SVA/NSM/nk/. The refractive index of protective TiO_2 from atomic layer deposition was obtained from spectroscopic ellipsometry. The Matlab function (*multidiel*), developed by Sophocles J. Orfanidis from Rutgers University, was used to calculate the reflection responses of the isotropic lossy multilayer dielectric structures [2]. The structural information used in the calculation is shown in Figure 1a.

UV-vis reflectance and transmittance measurement

The optical reflectance of the TiO_2 and Ni metal-coated TiO_2/III-V tandem substrates (Figure S3b) were determined by using an integrating sphere at normal incidence (Agilent Cary 5000 UV-Vis spectrometer). The absorptance (A) of TiO_2-coated tandem junction substrates was calculated from the measured total reflectance (R) and transmittance (T) of the electrode as $A = 1 - R - T$. All optical measurements were performed in air on fresh samples without chemical/electrochemical treatment. These results were used to select a TiO_2 anti-reflection coating thickness that increased current density in the current-limiting InGaP cell while still providing a thick conformal coverage of to serve as a protection layer.

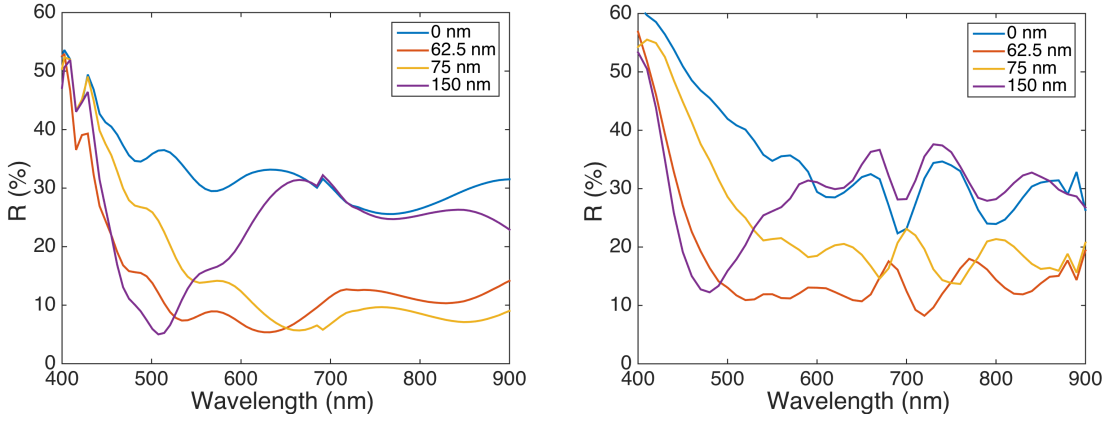

Figure S3. Reflectance of GaAs/InGaP structure with varying thicknesses of TiO_2 that serves as a single-layer anti-reflection coating. (a) Optical model. (b) Integrating sphere.

Discussion

External quantum yields of solid-state and PEC cells

The EQE of solid state and photoelectrochemical cells, shown in Fig. 1a and Fig. 2a, are not optimal and have room for improvement in future designs. Dual junction GaAs/InGaP devices in literature include double layer anti-reflection coatings (DLARCs) with optimized indices of refraction and thicknesses for a III-V layer stack. Many of these DLARCs are unstable in alkaline electrolyte or are unsuitable for operation in a planar PEC device. The solid-state measurements reported herein were obtained without any surface treatment or anti-reflection coating, which results in reflection losses of ~30% for most wavelengths in the solar spectrum. The behavior of the photoelectrode benefits slightly from being submerged in solution that has a higher index of refraction than air, as well as from the TiO_2 coating which acts as a (sub-optimal) single-layer anti-reflection coating (ARC). A second cause of reduced EQE is parasitic absorption by the 7 nm GaAs contact layer, which absorbs photons that have energies above the band gap of GaAs, 1.42 eV. The presence of this layer was needed to obtain facile for hole conduction through the TiO_2 protection layer, since ALD-TiO_2 grown on window layers that contained exposed aluminum did not exhibit the desired electrical properties. Simulations indicated that parasitic absorption of short wavelength light was especially detrimental to the performance of the high bandgap InGaP cell.

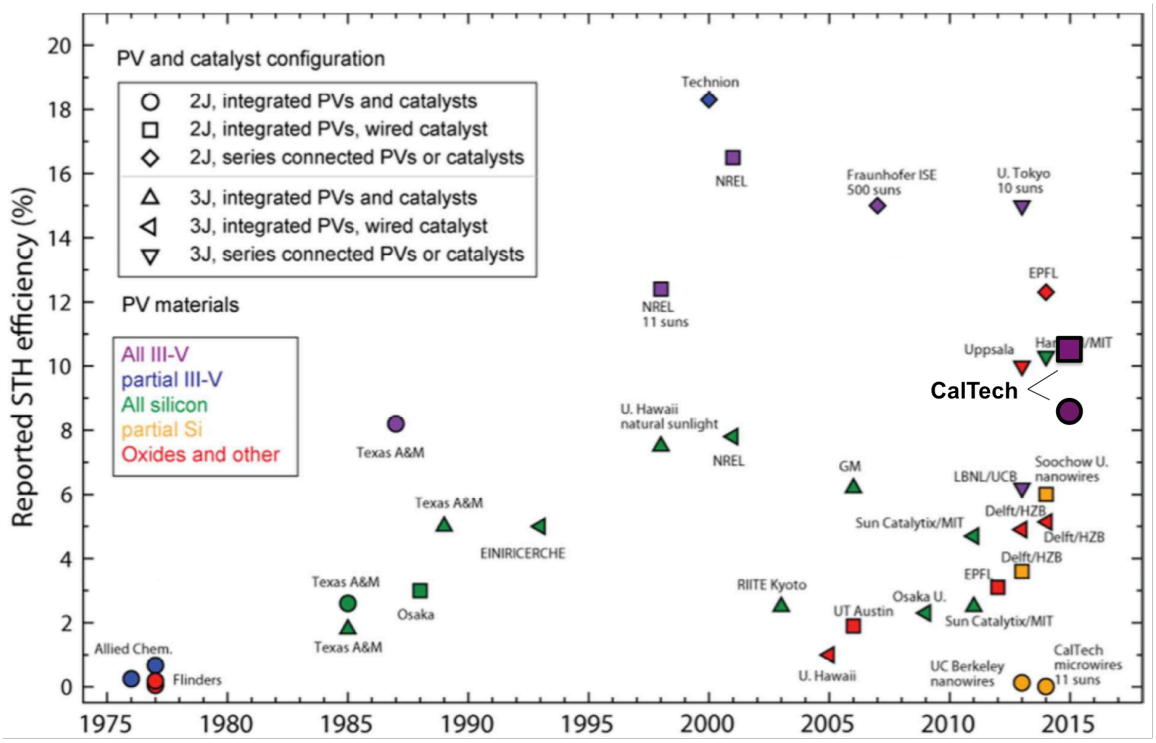

Figure S4. A compilation of reported solar-to-hydrogen (STH) efficiencies.[3] New entries (bold) indicate the efficiency of the 2J, integrated, III-V devices reported in the main text.

Operational Criteria for Safe, Efficient Electrolyzers:

Commercial electrolyzers must meet several criteria to be considered safe and reliable for operation and sale into the marketplace. They must be intrinsically safe, and not produce a flammable, potentially explosive mixture of $H_2(g)$ and $O_2(g)$ in the reactor at any point in space or time, especially because the reactor contains active catalysts for the recombination of the gases and is operating in the presence of light and heat. Electrolyzers must be able to withstand pressure differentials without undesirable crossover of gases or flooding and flow of the liquid electrolyte across the membrane separator, because the stoichiometry of the evolved H_2 and O_2 is 2:1. The membrane must be able to hold back pressure because a pressure differential is required to beneficially collect the $H_2(g)$ in a pipeline, as opposed to evolving the gas at atmospheric

pressure in a laboratory demonstration device. The photoelectrochemical systems described herein satisfy these same design and operational constraints in full.

Both modeling/simulation results and experimental data have shown that electrolyzers operated in solutions buffered to near-neutral pH are inefficient and/or not intrinsically safe. For example, operation of a membrane-free near-neutral pH a-Si:H device with ITO protective layers and earth-abundant, high overpotential electrocatalysts at $\eta_{STH} = 3.2\%$ produced 10% $O_2(g)$ in the cathode chamber and up to 40% $H_2(g)$ in the anode chamber, presenting an explosion hazard.[4] Introduction of a membrane was shown to yield a large reduction in the system efficiency and resulted in significant pH gradients near the electrode surfaces. Further modeling and simulation has shown that steady-state operation in such a geometry even in buffered solutions will result in pH gradients between the anode and cathode that produce local pH changes near the electrode surfaces, due to the consumption of protons associated with evolution of $H_2(g)$ from water and concomitant production of protons associated with production of $O_2(g)$ from H_2O.[4, 5] The overpotentials associated with the pH gradients and electrodialysis exceeded the combined overpotentials associated with the oxygen-evolving and hydrogen-evolving electrocatalysts, precluding the construction of an efficient (photo)electrolysis system. Further modeling and simulation efforts have shown that active convection by bubble evolution, for example, can minimize the formation of pH gradients but results in the loss of intrinsic safety, due to the concomitant co-evolution of stoichiometric, potentially explosive, mixtures of $H_2(g)$ and $O_2(g)$ at atmospheric pressure in the reaction vessel, in the presence of active catalysts for the recombination of these gases as well as in the presence of light and heat.[5]

Video

Full operation of the monolithically integrated 1 cm^2 prototype performing unassisted water splitting is available for download along with this publication.

1. J. R. McKone, B. F. Sadtler, C. A. Werlang, N. S. Lewis and H. B. Gray, *ACS Catalysis*, 2012, 3, 166-169.
2. S. J. Orfanidis, *Electromagnetic waves and antennas*, 2014.
3. J. W. Ager III, M. Shaner, K. Walczak, I. D. Sharp and S. Ardo, *Energy Environ. Sci.*, 2015, DOI: 10.1039/C5EE00457H.
4. J. Jin, K. Walczak, M. R. Singh, C. Karp, N. S. Lewis and C. X. Xiang, *Energy Environ. Sci.*, 2014, 7, 3371-3380.
5. M. R. Singh, K. M. Papadantonakis, C. Xiang and N. Lewis, *Energy Environ. Sci.*, 2015, DOI: 10.1039/C5EE01721A.